Interlayer superexchange in bilayer chromium trihalides

Kok Wee Song
Department of Physics and Astronomy, University of Exeter, Exeter, Devon EX4 4QL, United Kingdom

(Received 1 May 2023; accepted 9 June 2023; published 23 June 2023)

We construct a microscopic model based on superexchange theory for a moiré bilayer in chromium trihalides (CrX_3, $X = Br, I$). In particular, we derive analytically the interlayer Heisenberg exchange and the interlayer Dzyaloshinskii-Moriya interaction with arbitrary distances ($\boldsymbol{x}$) between spins. Importantly, our model takes into account sliding and twisting geometries in the interlayer X-X hopping processes. Our approach can directly access the $\boldsymbol{x}$-dependent interlayer exchange without large unit-cell calculations. We argue that deducing interlayer exchange by various sliding bilayers may lead to an incomplete result in a moiré bilayer. Using the *ab initio* tight-binding Hamiltonian, we numerically evaluate the exchange interactions in CrI_3. We find that our analytical model agrees with previous comprehensive density functional theory studies. Furthermore, our findings reveal the important role of the correlation effects in the X's p orbitals, which give rise to a rich interlayer magnetic interaction with remarkable tunability.

DOI: 10.1103/PhysRevB.107.245133

I. INTRODUCTION

Two-dimensional (2D) magnetism in CrX_3 [1–6] exhibits many fascinating phenomena such as topological magnons [7–13], moiré magnetism [14–24], and Kitaev physics [25–29]. Interestingly, CrX_3 may serve as a magnetic building block in forming van der Waal heterostructures [30,31] for spintronic applications [32–40]. Furthermore, the material's unique interlayer exchange coupling is highly tunable leading to intriguing stacking-dependent magnetism [41–50]. In this regard, it has recently attracted much research interest [51–60], particularly in its moiré lattice. Studying these magnetic 2D materials may require comprehensive *ab initio* modeling that can be challenging in a large moiré cell. Therefore, an analytical model that can evaluate the spin Hamiltonian accurately is highly desirable. However, this demands an understanding of the interlayer exchange at the microscopic level. Nevertheless, the microscopic origin of the material's interlayer antiferromagnetic (AFM) exchange and its competition with the interlayer ferromagnetic (FM) exchange [53,54] remains elusive in theory and experiment.

Investigating the interlayer exchange in a CrX_3 moiré bilayer is a nontrivial theoretical problem since the exchange coupling mediated by Cr-X-X-Cr hopping is a complicated process [51] [Fig. 1(d)]. Moreover, studying the noncollinear spin order due to the interlayer Dzyaloshinskii-Moriya (DM) interaction induced by spin-orbit coupling (SOC) is also an outstanding question in this moiré bilayer. In this paper, we focus on tackling these problems by developing a microscopic model using the superexchange theory [61–63]. In our model, we show that the AFM exchange stems from the hopping processes involving the correlated virtual hole pair in the X ion. Also, we will demonstrate that our analytical model yields an accurate spin Hamiltonian for a moiré bilayer by performing a small-scale density functional theory (DFT) simulation.

II. MODEL

To study the magnetic ground state, we model the bilayer CrX_3 on-site Hamiltonian [63] as

$$\mathcal{H}_0 = \sum_{\ell=1,2}\sum_{\mathbf{R}=\mathbf{r},\dot{\mathbf{r}}}\sum_{\alpha\alpha'}\left\{\left[\epsilon^{\alpha}_{\mathbf{R}}\delta_{\alpha\alpha'} + U^{\alpha\alpha'}_{\mathbf{R}}\left(\hat{n}^{\ell}_{\mathbf{R}\alpha'} - \frac{1}{2}\delta_{\alpha\alpha'}\right)\right]\hat{n}^{\ell}_{\mathbf{R}\alpha} - J^{\alpha\alpha'}_{\mathbf{R}}\hat{\mathbf{s}}^{\ell}_{\mathbf{R}\alpha}\cdot\hat{\mathbf{s}}^{\ell}_{\mathbf{R}\alpha'}\right\}, \tag{1}$$

where, in each layer ℓ, the X's and Cr's in-plane positions are labeled by $\mathbf{r}$ and $\dot{\mathbf{r}}$. The occupation number and the spin angular momentum operators are

$$\left(\hat{n}^{\ell}_{\mathbf{R}\alpha}, \hat{\mathbf{s}}^{\ell}_{\mathbf{R}\alpha}\right) = \frac{1}{2}\begin{cases} d^{\ell\dagger}_{\dot{\mathbf{r}}\dot{\alpha}\sigma}(\delta_{\sigma\sigma'}, \boldsymbol{\tau}_{\sigma\sigma'})d^{\ell}_{\dot{\mathbf{r}}\dot{\alpha}\sigma'}, & \dot{\alpha} = 1\ldots5, \\ p^{\ell\dagger}_{\mathbf{r}\alpha\sigma}(\delta_{\sigma\sigma'}, \boldsymbol{\tau}_{\sigma\sigma'})p^{\ell}_{\mathbf{r}\alpha\sigma'}, & \alpha = \tilde{x}, \tilde{y}, \tilde{z}, \end{cases}$$

where $p^{\ell\dagger}_{\mathbf{r}\alpha\sigma}$ and $d^{\ell\dagger}_{\dot{\mathbf{r}}\dot{\alpha}\sigma}$ are the creation field operators for p and d orbitals with orbital indices α and $\dot{\alpha}$. Here, σ is the spin index which is quantized in the out-of-plane (z) direction and $\boldsymbol{\tau} = (\tau^x, \tau^y, \tau^z)$ are the Pauli matrices. We note that we use the dotted and undotted indices to explicitly distinguish between d and p orbitals. The model parameter $\epsilon^{\alpha}_{\mathbf{R}}$ is the on-site energy, and $U^{\alpha\alpha'}_{\mathbf{R}}, J^{\alpha\alpha'}_{\mathbf{R}} > 0$ are the on-site Coulomb and Hund interacting constants. The tight-binding (TB) Hamiltonian is

$$\mathcal{H}' = \sum_{\ell\dot{1}1}\left(t_{\dot{1}1}p^{\ell\dagger}_{1\sigma}d^{\ell}_{\dot{1}\sigma} + t_{\dot{1}1}d^{\ell\dagger}_{\dot{1}\sigma}p^{\ell}_{1\sigma}\right) + \sum_{\ell\dot{1}\dot{2}}u_{\dot{1}\dot{2}}d^{\ell\dagger}_{\dot{1}\sigma}d^{\ell}_{\dot{2}\sigma} + \sum_{\ell\ell',12}\left[(v_{12}\delta_{\sigma\sigma'} + \boldsymbol{\Lambda}_{12}\cdot\boldsymbol{\tau}_{\sigma\sigma'})\delta_{\ell\ell'} + T^{\ell\ell'}_{12}\delta_{\sigma\sigma'}\right]p^{\ell\dagger}_{1\sigma}p^{\ell'}_{2\sigma'}, \tag{2}$$

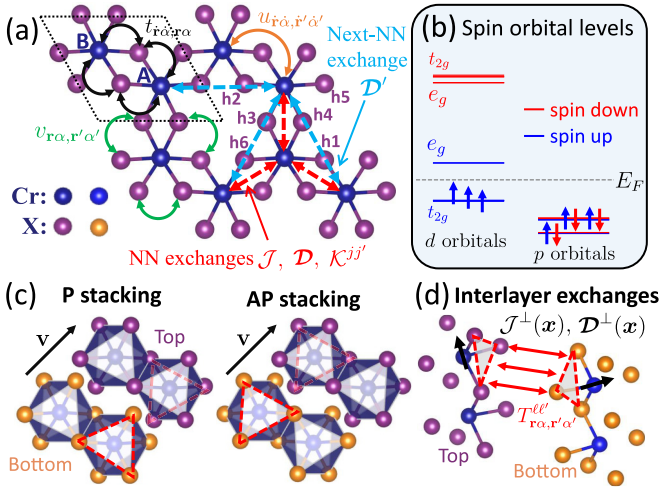

FIG. 1. Intralayer and interlayer couplings. (a) Monolayer CrX_3 with hopping constants, $t_{\dot{\mathbf{r}}\dot{\alpha},\mathbf{r}\alpha}$, $u_{\dot{\mathbf{r}}\dot{\alpha},\dot{\mathbf{r}}'\dot{\alpha}'}$, and $v_{\mathbf{r}\alpha,\mathbf{r}'\alpha'}$, and intralayer exchanges, $\mathcal{J}$ (Heisenberg), $\boldsymbol{\mathcal{D}}$, $\boldsymbol{\mathcal{D}}'$ (DM), and $\mathcal{K}^{jj'}$(symmetric). For each unit cell (dashed parallelogram), it contains two Cr sublattices A and B. (b) The orbital levels for spin-up and spin-down states with Fermi energy E_F. (c) The unit cell of a parallel (P) stacking in bilayer CrX_3 (displaced by $\mathbf{v}$ for clarity). Antiparallel (AP) stacking is obtained by rotating the bottom layer by $\pi/3$. (d) The interlayer exchanges $\mathcal{J}^{\perp}$ and $\boldsymbol{\mathcal{D}}^{\perp}$ are mediated by the hopping between the X ions located in the two red dashed triangles.

where we used the shorthand notation $n \equiv (\mathbf{r}_n\alpha_n)$ and $\dot{n} \equiv (\dot{\mathbf{r}}_n\dot{\alpha}_n)$ to represent the position and the orbital index for p and d orbitals. The intralayer nearest-neighbor (NN) and next-NN hopping constants are $t_{1\dot{1}}$, $u_{\dot{1}\dot{2}}$, and v_{12} [Fig. 1(a)]. The SOC is written in vector form $\boldsymbol{\Lambda}_{12} = -i\lambda\sum_{\alpha}\boldsymbol{p}^{\alpha}_{\mathbf{r}_1}\varepsilon_{\alpha\alpha_2\alpha_1}\delta_{\mathbf{r}_2\mathbf{r}_1}$ with coupling strength λ and Levi-Civita symbol $\varepsilon_{\alpha\alpha_2\alpha_1}$. We remark that the p-orbital quantization axes $\boldsymbol{p}^{\tilde{x},\tilde{y},\tilde{z}}_{\mathbf{r}}$ ($|\boldsymbol{p}^{\alpha}_{\mathbf{r}}| = 1$) are not arbitrary due to the crystal-field splitting [63].

III. SUPEREXCHANGE THEORY

The magnetic properties are mostly determined by the low-energy excitations in the Mott's insulating ground state [61,62]. The Mott's state has the many-body wave function

$$|\tilde{\Psi}\rangle = \prod_{\ell\dot{\mathbf{r}},\dot{\alpha}\leqslant 3}\chi^{\ell+}_{\dot{\mathbf{r}}\sigma}d^{\ell\dagger}_{\dot{\mathbf{r}}\dot{\alpha}\sigma}\prod_{\ell\mathbf{r}\alpha}p^{\ell\dagger}_{\mathbf{r}\alpha\uparrow}p^{\ell\dagger}_{\mathbf{r}\alpha\downarrow}|0\rangle, \tag{3}$$

where $(\chi^{\ell+}_{\dot{\mathbf{r}}\uparrow}, \chi^{\ell+}_{\dot{\mathbf{r}}\downarrow}) = (1+s^{\ell}_{\dot{\mathbf{r}}z}, s^{\ell}_{\dot{\mathbf{r}}x} + is^{\ell}_{\dot{\mathbf{r}}y})/\sqrt{2(1+s^{\ell}_{\dot{\mathbf{r}}z})}$ is the local spin wave function pointing in $\mathbf{s}^{\ell}_{\dot{\mathbf{r}}} = (s^{\ell}_{\dot{\mathbf{r}}x}, s^{\ell}_{\dot{\mathbf{r}}y}, s^{\ell}_{\dot{\mathbf{r}}z})$ with $|\mathbf{s}^{\ell}_{\dot{\mathbf{r}}}| = 1$ [64]. In the Mott's state, the p orbitals are filled while the d orbitals are half filled in t_{2g} ($\dot{\alpha} = 1, 2, 3$) and empty in e_g [$\dot{\alpha} = 4, 5$, Fig. 1(b)]. Because of Hund's interaction, in Eq. (3), all the spins at $\dot{\mathbf{r}}$ are deemed to be parallel with $\mathbf{s}^{\ell}_{\dot{\mathbf{r}}}$.

The grand partition function for Mott's state in the interacting picture (treating $\mathcal{H}'$ as a perturbation) is

$$\mathcal{Z} = \sum_{\tilde{\Psi}}\langle\tilde{\Psi}|\mathcal{T}e^{-\int_0^{\beta}d\tau\mathcal{H}'(\tau)}|\tilde{\Psi}\rangle \approx \sum_{\text{all possible }\mathbf{s}_{\dot{\mathbf{r}}}}\exp(-\beta H_s),$$

where $\sum_{\tilde{\Psi}}$ represents the sum in the functional space of the many-body wave function $\tilde{\Psi} = \prod_{\ell\dot{\mathbf{r}},\dot{\alpha}\leqslant 3}\chi^{\ell+}_{\dot{\mathbf{r}}\sigma}$. Here, $\mathcal{T}$ is the time-order operator and $\mathcal{H}'(\tau) = e^{\tau\mathcal{H}_0}\mathcal{H}'e^{-\tau\mathcal{H}_0}$ with τ being the imaginary time. Here, β is the inverse of temperature. At low temperature, this perturbation expansion [63,65] (seventh order) leads to

$$H_s = \sum_{\ell}\left[\sum_{\langle\dot{\mathbf{r}}\dot{\mathbf{r}}'\rangle}\left(\mathcal{J}\mathbf{S}^{\ell}_{\dot{\mathbf{r}}}\cdot\mathbf{S}^{\ell}_{\dot{\mathbf{r}}'} + \boldsymbol{\mathcal{D}}_{\dot{\mathbf{r}}\dot{\mathbf{r}}'}\cdot\mathbf{S}^{\ell}_{\dot{\mathbf{r}}}\times\mathbf{S}^{\ell}_{\dot{\mathbf{r}}'} + \sum_{jj'}^{x,y,z}S^{\ell}_{\dot{\mathbf{r}}j}\mathcal{K}^{jj'}_{\dot{\mathbf{r}}\dot{\mathbf{r}}'}S^{\ell}_{\dot{\mathbf{r}}'j'}\right) + \sum_{\langle\langle\dot{\mathbf{r}}\dot{\mathbf{r}}'\rangle\rangle}\boldsymbol{\mathcal{D}}'_{\dot{\mathbf{r}}\dot{\mathbf{r}}'}\cdot\mathbf{S}^{\ell}_{\dot{\mathbf{r}}}\times\mathbf{S}^{\ell}_{\dot{\mathbf{r}}'} + \sum_{\ell'\neq\ell}^{\ell'\neq\ell}\left(\mathcal{J}^{\perp}_{\dot{\mathbf{r}}\dot{\mathbf{r}}'}\mathbf{S}^{\ell}_{\dot{\mathbf{r}}}\cdot\mathbf{S}^{\ell'}_{\dot{\mathbf{r}}'} + \boldsymbol{\mathcal{D}}^{\perp}_{\dot{\mathbf{r}}\dot{\mathbf{r}}'}\cdot\mathbf{S}^{\ell}_{\dot{\mathbf{r}}}\times\mathbf{S}^{\ell'}_{\dot{\mathbf{r}}'}\right)\right], \tag{4}$$

with $\mathbf{S}^{\ell}_{\dot{\mathbf{r}}} = \frac{3}{2}\mathbf{s}^{\ell}_{\dot{\mathbf{r}}}$. In the spin Hamiltonian H_s, the first three terms are the intralayer NN exchange between AB sublattices [Fig. 1(a)]. The fourth term is the intralayer NN exchange between AA/BB sublattices. The last two terms are the interlayer Heisenberg exchange $\mathcal{J}^{\perp}_{\dot{\mathbf{r}}\dot{\mathbf{r}}'}$ and interlayer DM interaction $\boldsymbol{\mathcal{D}}^{\perp}_{\dot{\mathbf{r}}\dot{\mathbf{r}}'}$ which are relevant to the moiré magnetism. The derivation of these interlayer exchanges can be found in the Supplemental Material [66] (SM) and we summarized their analytical expression as follows,

$$\mathcal{J}^{\perp}_{\dot{\mathbf{r}}_1\dot{\mathbf{r}}_2} = \frac{2^2}{3^2}\frac{t_{\dot{1}1}t_{4\dot{1}}}{2\mathcal{E}_{\dot{1}1}\mathcal{E}_{\dot{1}4}}\left\{\frac{P_{\dot{\alpha}_2}T^{\ell_2\ell_1}_{34}t_{\dot{2}3}T^{\ell_1\ell_2}_{12}t_{2\dot{2}}}{\mathcal{E}_{\dot{1}2}\mathcal{E}_{\dot{1}3}(\omega_{\dot{1}}-\bar{\omega}_{\dot{2}})} - \frac{t_{\dot{2}3}T^{\ell_1\ell_2}_{12}-\xi t_{\dot{2}2}T^{\ell_1\ell_2}_{13}}{2(\mathcal{E}_{\dot{1}3}+\mathcal{E}_{\dot{2}2}+\Theta^{\xi}_{23})}\left[\frac{t_{2\dot{2}}T^{\ell_2\ell_1}_{34}}{\mathcal{E}^2_{\dot{1}3}} + \frac{t_{2\dot{2}}T^{\ell_2\ell_1}_{34}}{\mathcal{E}^2_{\dot{2}2}}\right]\right\}, \quad P_{\dot{\alpha}} = \begin{cases}1, & \dot{\alpha}\leqslant 3\\ 0, & \dot{\alpha}>3\end{cases}; \tag{5}$$

$$\boldsymbol{\mathcal{D}}^{\perp}_{\dot{\mathbf{r}}_1\dot{\mathbf{r}}_2} = i\frac{2^2}{3^2}\frac{t_{\dot{1}1}t_{5\dot{1}}}{\mathcal{E}_{\dot{1}1}\mathcal{E}_{\dot{1}5}}\left\{\frac{P_{\dot{\alpha}_2}T^{\ell_2\ell_1}_{45}t_{\dot{2}4}\left[T^{\ell_1\ell_2}_{12}\boldsymbol{\Lambda}_{23}+\boldsymbol{\Lambda}_{12}T^{\ell_1\ell_2}_{23}\right]t_{3\dot{2}}}{(\omega_{\dot{1}}-\bar{\omega}_{\dot{2}})\mathcal{E}_{\dot{1}2}\mathcal{E}_{\dot{1}3}\mathcal{E}_{\dot{1}4}} + \frac{T^{\ell_2\ell_1}_{45}t_{\dot{2}2}\left(\frac{1}{\mathcal{E}_{\dot{2}2}}-\frac{1}{\mathcal{E}_{\dot{1}4}}\right)+\xi T^{\ell_2\ell_1}_{25}t_{4\dot{2}}\left(\frac{1}{\mathcal{E}_{\dot{2}4}}-\frac{1}{\mathcal{E}_{\dot{1}2}}\right)}{\left(\mathcal{E}_{\dot{1}2}+\mathcal{E}_{\dot{2}4}+\Theta^{\xi}_{24}\right)}\left[\frac{T^{\ell_1\ell_2}_{14}t_{\dot{2}3}\boldsymbol{\Lambda}_{32}}{\mathcal{E}_{\dot{2}3}(\mathcal{E}_{\dot{1}1}+\mathcal{E}_{\dot{2}2})}\right.\right.$$

$$\left.\left. - \frac{T^{\ell_1\ell_2}_{34}t_{\dot{2}2}\boldsymbol{\Lambda}_{13}}{\mathcal{E}_{\dot{2}2}(\mathcal{E}_{\dot{1}3}+\mathcal{E}_{\dot{2}2})} - \xi\frac{\left(T^{\ell_1\ell_2}_{13}\boldsymbol{\Lambda}_{32}+\boldsymbol{\Lambda}_{13}T^{\ell_1\ell_2}_{32}\right)t_{\dot{2}4}}{\mathcal{E}_{\dot{1}2}\mathcal{E}_{\dot{1}3}} + \frac{\boldsymbol{\Lambda}_{34}}{2}\frac{T^{\ell_1\ell_2}_{12}t_{\dot{2}3}\left(\frac{1}{\mathcal{E}_{\dot{1}2}}-\frac{1}{\mathcal{E}_{\dot{2}3}}\right)+\xi T^{\ell_1\ell_2}_{13}t_{\dot{2}2}\left(\frac{1}{\mathcal{E}_{\dot{2}2}}-\frac{1}{\mathcal{E}_{\dot{1}3}}\right)}{\left(\mathcal{E}_{\dot{1}2}+\mathcal{E}_{\dot{2}3}+\Theta^{-\xi}_{23}\right)}\right]\right\}, \tag{6}$$

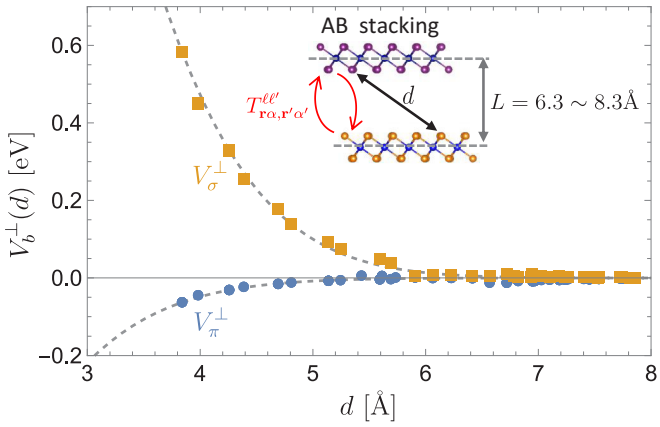

FIG. 2. Koster-Slater parameters. The dashed curves are fitted by using Eq. (7). The KS integral is obtained by the DFT calculation with the AB-stacking bilayer (P stacking). The interlayer distance increases in steps of 0.5 Å.

where the sums of all indices are implicitly assumed except $\dot{\mathbf{r}}_{1,2}$. In the above, $\omega_{\dot{n}}$ ($\bar{\omega}_{\dot{n}}$) is the energy for creating a quasielectron (quasihole) in the d orbitals with a spin wave function $\chi^{\ell+}_{\dot{\mathbf{r}}\sigma}$. Namely, the quasielectron (quasihole) state is $|\dot{n}\rangle = \chi^{\ell+}_{\dot{\mathbf{r}}_n\sigma} d^{\ell\dagger}_{\dot{n}\sigma}|\tilde{\Psi}\rangle$ ($|\underline{\dot{n}}\rangle = \bar{\chi}^{\ell+}_{\dot{\mathbf{r}}_n\sigma} d^{\ell}_{\dot{n}\sigma}|\tilde{\Psi}\rangle$) with $\mathcal{H}_0|\dot{n}\rangle = \omega_{\dot{n}}|\dot{n}\rangle$. Furthermore, $\mathcal{E}_{\dot{n}n}$ is the creation energy of a d-electron and p-hole pair, $|\dot{n}n\rangle = \bar{\chi}^{\ell+}_{\dot{\mathbf{r}}_n\sigma'} p^{\ell}_{n\sigma'}|\dot{n}\rangle$, with $\mathcal{H}_0|\dot{n}n\rangle = \mathcal{E}_{\dot{n}n}|\dot{n}n\rangle$. Similarly, the two electron-hole pairs are $|\dot{m}m,\dot{n}n\rangle_\xi = \bar{\chi}^{\ell+}_{\dot{\mathbf{r}}_m\sigma'}\bar{\chi}^{\ell+}_{\dot{\mathbf{r}}_n\sigma''}(p^{\ell}_{m\sigma'}p^{\ell}_{n\sigma''} + \xi\, p^{\ell}_{m\sigma''}p^{\ell}_{n\sigma'})|\dot{m}\dot{n}\rangle$ where $\xi = \pm 1$ for a spin triplet/singlet state with energy $\mathcal{H}_0|\dot{m}m,\dot{n}n\rangle_\xi = (\mathcal{E}_{\dot{m}m} + \mathcal{E}_{\dot{n}n} + \Theta^{\xi}_{mn})|\dot{m}m,\dot{n}n\rangle_\xi$. The spin singlet-triplet energy splitting due to an interaction is given by $\Theta^{\xi}_{mn} = \frac{1}{2}[U^{\alpha_m\alpha_n}_{\mathbf{r}_m} - (2\xi+1)(1-\delta_{\alpha_m\alpha_n})J^{\alpha_m\alpha_n}_{\mathbf{r}_m}]\delta_{\mathbf{r}_m\mathbf{r}_n}$. For simplicity, in Eqs. (5) and (6), the high-energy virtual states in the d orbitals [66] [spin-down states in Fig. 1(b)] are projected out [63]. For calculating the exchange coupling of any two spins, we consider only the first nine shortest paths for the interlayer X-X hopping which is depicted in Fig. 1(d).

IV. INTERLAYER EXCHANGE IN CrI_3

To estimate the interlayer exchange coupling, we model the interlayer hopping as

$$T^{\ell\ell'}_{\mathbf{r}\alpha,\mathbf{r}'\alpha'} = \delta_{\alpha\alpha'}V^{\perp}_{\pi} + (V^{\perp}_{\sigma} - V^{\perp}_{\pi})\frac{\boldsymbol{p}^{\alpha}_{\mathbf{r}}\cdot\boldsymbol{d}\,\boldsymbol{p}^{\alpha'}_{\mathbf{r}'}\cdot\boldsymbol{d}}{d^2}, \tag{7}$$

where $\boldsymbol{d} = \mathbf{r} + \mathbf{h}_\ell - (\mathbf{r}' + \mathbf{h}_{\ell'})$ is the displacement between two X ions with $\mathbf{h}_{1,2} = \pm\frac{1}{2}(0,0,L)$. Here, L is the interlayer distance between Cr planes (Fig. 2). The Slater-Koster (SK) overlap integral is parametrized [67] by a $\boldsymbol{d}$-dependent function as

$$V^{\perp}_b = \nu_b \exp[-(d/R_b)^{\xi_b}], \quad b = \pi, \sigma. \tag{8}$$

To find the SK parameters ν_b, R_b, and ξ_b, we compute $T^{\ell\ell'}_{\mathbf{r}\alpha,\mathbf{r}'\alpha'}$ by constructing an *ab initio* TB Hamiltonian using QUANTUM ESPRESSO [68], WANNIER90 [69,70], and the pseudopotential from the standard solid-state pseudopotential efficiency library [71,72] (see SM [66]). We then perform the fitting (Fig. 2) for the SK parameters [73] by using $T^{\ell\ell'}_{\mathbf{r}\alpha,\mathbf{r}'\alpha'}$ with various interlayer distances ($L = 6.3$–8.3 Å) and the result is summarized in Table I.

TABLE I. Koster-slater integral $V^{\perp}_b = \nu_b \exp[-(d/R_b)^{\xi_b}]$ for interlayer hopping.

b	ν_b	R_b	ξ_b
σ	5.3547	2.6794	2.2148
π	−2.3698	1.7993	1.7021

We then proceed to obtain the TB constants and $\boldsymbol{p}^{\alpha}_{\mathbf{r}}$ in $\mathcal{H}'$ by extracting them from the spin-up *ab initio* TB Hamiltonian. Using the spin-down TB constants only leads to minor modifications [63]. However, we note that the correlation energy Θ^{ξ}_{nn} cannot be obtained by the one-particle Kohn-Sham spectrum. Therefore, the interactions between p holes, $U^{\alpha\alpha'}_{\mathbf{r}_n}$ and $J^{\alpha\alpha'}_{\mathbf{r}_n}$, remain free parameters in our model. Here, we use $U^{\alpha\alpha'}_{\mathbf{r}_n} = 1.2$ eV and $J^{\alpha\alpha'}_{\mathbf{r}_n} = 0.5$ eV from Ref. [63]. Once all the model parameters are determined, we can calculate the superexchange in Eqs. (5) and (6). But, the quasiparticle energies between the spin-up t_{2g} (valence) and e_g (conduction) bands [Fig. 1(b)] in the *ab initio* TB Hamiltonian are inaccurate due to the band-gap underestimation in DFT [63]. To correct this, it requires performing a GW calculation [74,75] which is beyond the scope of this paper. Instead, we employ the "scissor" correction [76–79] by rigidly shifting the conduction e_g bands by an additional 1.2 eV [66] above the valence t_{2g} band to match the intralayer exchange [80–86], $\mathcal{J} \sim 4$ meV.

To investigate our model, we analyze the isotropic exchange $\mathcal{J}^{\perp}_{\dot{\mathbf{r}}\dot{\mathbf{r}}'}$ with arbitrary in-plane displacement $\boldsymbol{x} = \dot{\mathbf{r}} - \dot{\mathbf{r}}'$ (with $L = 6.8$ Å). In Fig. 3, we plot two different types of superexchange, SE1 and SE2 (left panel). They both contribute to $J^{\perp}_{\dot{\mathbf{r}}\dot{\mathbf{r}}'}$. In the superexchange hopping processes, SE1 creates only *one* virtual p hole ($|\dot{n}n\rangle$) while SE2 creates *two* virtual p holes ($|\dot{m}m,\dot{n}n\rangle_\xi$). In contrast to the previous studies, we go beyond the SE1 process and we find that the interlayer AFM exchange is mostly mediated by a virtual singlet hole pair through the e_g-e_g hopping process in SE2 [63]. As we can see, SE1 mediates mostly FM exchange which cannot explain the emergence of AFM exchange. Combining SE1 and SE2 gives the total interlayer exchange whose result agrees with the comprehensive DFT calculation in Refs. [22,24]. Similarly, we calculate the interlayer DM interaction in Fig. 4. In P stacking [Fig. 1(c)], at $\boldsymbol{x} = \mathbf{0}$, we find that $\boldsymbol{\mathcal{D}}^{\perp}(0)$ has zero in-plane components due to threefold rotational symmetry [87]. However, in AP stacking, we find that $\boldsymbol{\mathcal{D}}^{\perp}(0)$ [87] vanishes since it has an additional mirror symmetry between the top and bottom layers. Similar to $\mathcal{J}^{\perp}_{\dot{\mathbf{r}}\dot{\mathbf{r}}'}$, we also find that SE1 and SE2 have comparable contributions for $\boldsymbol{\mathcal{D}}^{\perp}_{\dot{\mathbf{r}}\dot{\mathbf{r}}'}$. Furthermore, our theory can also derive the analytical form for the intralayer next-NN DM interaction [88] $\boldsymbol{\mathcal{D}}'$ and the NN symmetric exchange tensor [89] $\mathcal{K}^{ij}$. These higher-order intralayer exchanges are relevant for topological magnetic phenomena [7–13] and Kitaev physics [25–29].

V. MAGNETIC MOIRÉ BILAYER

As demonstrated in previous work [20,21,23,24], $\mathcal{J}^{\perp}_{\dot{\mathbf{r}}\dot{\mathbf{r}}'}$ can also be deduced by mapping the local Cr-Cr stacking order in

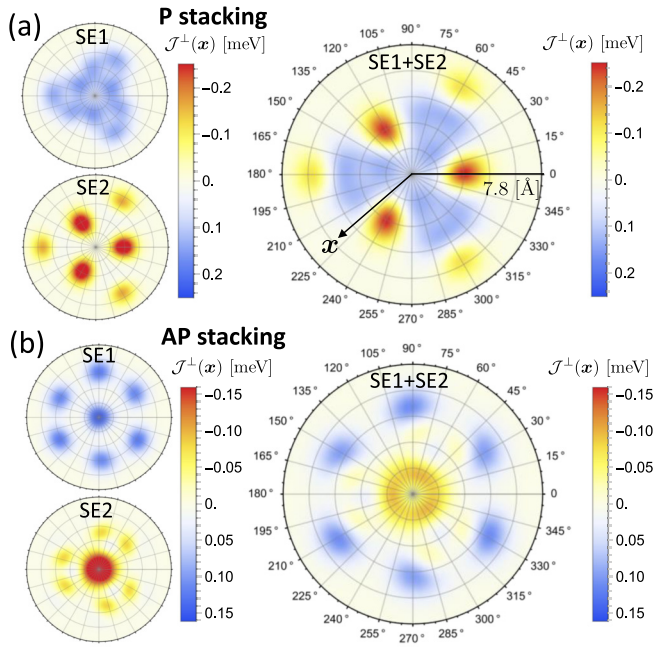

FIG. 3. Interlayer exchange coupling. The dependence of $\boldsymbol{x} = \dot{\mathbf{r}} - \dot{\mathbf{r}}'$ in the interlayer exchange coupling $\mathcal{J}^{\perp}(\boldsymbol{x})$ between spins at in-plane positions $\dot{\mathbf{r}}$ and $\dot{\mathbf{r}}'$. (a) The exchange coupling between AA sublattices in P stacking [see Fig. 1(c)]. The left panel shows the separate contributions from SE1 and SE2 processes. The right panel is the total exchange coupling. (b) The exchange coupling between AA sublattices in AP stacking.

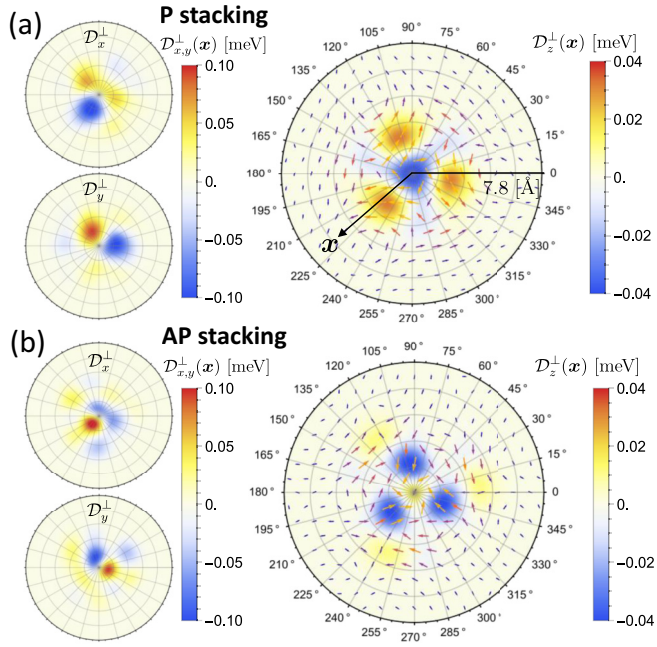

FIG. 4. Interlayer DM interaction. (a) Interlayer DM interaction between AA sublattices for P stacking. The left panel is the coupling strength for $\mathcal{D}_x^{\perp}$ and $\mathcal{D}_y^{\perp}$ components. In the right panel, the vector field shows the in-plane component of the DM interaction. The out-of-plane component is illustrated by the color plot. (b) Interlayer DM interaction between AA sublattices in AP stacking.

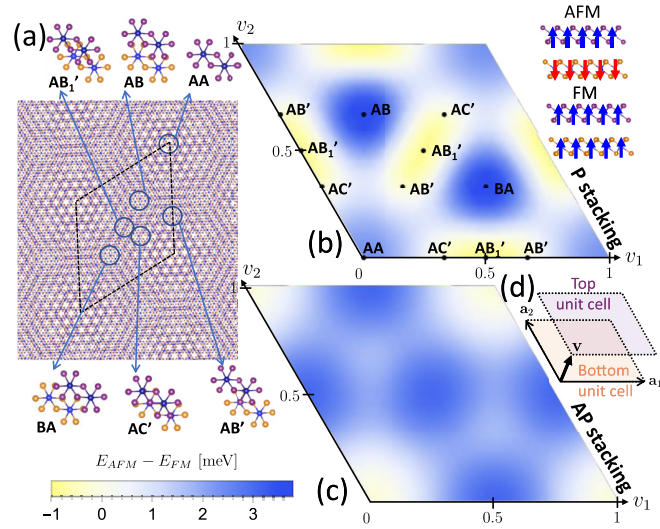

FIG. 5. Moiré field. (a) The mapping between the local stacking order in a moiré lattice and the bilayer stacking with various sliding vectors $\mathbf{v}$. (b) The moiré field for P stacking is obtained by using Eqs. (4) and (5), and setting $\mathcal{K}^{jj'} = 0$. (c) The moiré field for AP stacking. (d) The unit cells in different layers with the sliding vector $\mathbf{v} = v_1\mathbf{a}_1 + v_2\mathbf{a}_2$.

a moiré cell to the corresponding sliding bilayer [Fig. 5(a)]. In this "sliding-mapping" approach [24], the DFT calculation is performed in the sliding bilayer instead of the twisted bilayer with a large moiré cell. To compare our model with this approach, we calculate $E_{\rm AFM} - E_{\rm FM} = \frac{2}{N}\sum_{\dot{\mathbf{r}}\dot{\mathbf{r}}'}(\mathcal{J}^{\perp}_{\dot{\mathbf{r}}\dot{\mathbf{r}}'} + \mathcal{J}^{\perp}_{\dot{\mathbf{r}}'\dot{\mathbf{r}}})(\frac{3}{2})^2$ for a bilayer with N unit cells where $E_{\rm AFM}$ and $E_{\rm FM}$ are the total energies per unit cell in layered-AFM and FM states. The result is plotted as a "moiré field" [21] with a sliding vector $\mathbf{v}$ in Figs. 5(b) and 5(c). Even though our model is constructed based on five DFT data points on the AB stacking (Fig. 2), our result in Fig. 5 agrees with the comprehensive DFT studies [20,21,51,55]. We note that the AFM domain has a slight mismatch with a smaller energy gain as compared to the other DFT studies. This discrepancy may be attributed to the lack of variation of $\boldsymbol{p}_{\mathbf{r}}^{\alpha}$ in response to the change of local crystal field in different stacking structures. This is especially evident for the AP stacking moiré field [Fig. 5(c)], as we use Eq. (7) deduced from AB stacking (Fig. 2) in the calculation. In superexchange theory, the interlayer exchange is expected to strongly depend on the details of $\boldsymbol{p}_{\mathbf{r}}^{\alpha}$, since it governs the overlapping between p orbitals [90,91].

VI. CONCLUSION

We have built a microscopic spin Hamiltonian for a moiré bilayer by using the superexchange theory. Although the construction is done by a relatively small DFT simulation, our analytical model yields a similar result as compared to the rigorous DFT studies. Furthermore, we identify the microscopic origin of the interlayer AFM exchange. This exchange is mediated by the singlet hole pairs in the X's ion [63]. These low-energy SE2 processes play a vital role in interlayer exchanges.

In superexchange, the interlayer exchange coupling is highly sensitive to the interlayer X-X hopping geometry, which can lead to different $\boldsymbol{x}$-dependent behavior in twisting (see P and AP stackings in Figs. 3 and 4). In the sliding-mapping approach [20,21,51,55], the moiré fields in P and AP stackings [55] [Figs. 5(b) and 5(c)] will generate two different $\mathcal{J}^{\perp}(\boldsymbol{x})$. Also, P and AP stackings do not transform into each other by sliding since this does not introduce a relative rotation between X planes [92]. Hence, the sliding method may not realize all the relevant interlayer exchange coupling in a twisted bilayer. Therefore, we argue that our microscopic approach can complement the incomplete part of the sliding method.

In our theory, the KS parametrization in Eq. (7) may not be sufficient since it does not take into account the variation of the p-orbital quantization axes in different crystal-field environments. To improve our model by including such effects, it requires more DFT simulations with different stacking configurations. This is particularly important for evaluating anisotropic exchanges such as interlayer DM interactions. Another limitation of our approach is that the Coulomb and Hund's interaction in the p orbital cannot be obtained from the DFT Kohn-Sham spectrum since this information is contained in the two-particle spectrum. This may require further effort in evaluating the two-particle spectrum from first-principles studies.

In conclusion, our work provides microscopic insights into the problem of interlayer magnetic exchange interactions. Unlike conventional bulk materials, the p-orbital wave functions do not have symmetry constraints in the out-of-plane direction. Owing to the absence of this crystalline symmetry, this unique property in 2D materials leads to a fascinatingly rich stacking-dependent magnetism with remarkable tunability.

ACKNOWLEDGMENTS

The author would like to thank Marco Berritta and Stefano Scali for stimulating discussions. The author also thanks Oleksandr Kyriienko and Vladimir Fal'ko for supporting this work through scientific guidance. The author acknowledges the financial support from U.K. EPSRC New Investigator Award under Agreement No. EP/V00171X/1.

[1] M. A. McGuire, H. Dixit, V. R. Cooper, and B. C. Sales, Coupling of crystal structure and magnetism in the layered, ferromagnetic insulator CrI_3, Chem. Mater. **27**, 612 (2015).

[2] K. S. Burch, D. Mandrus, and J.-G. Park, Magnetism in two-dimensional van der Waals materials, Nature (London) **563**, 47 (2018).

[3] M. Gibertini, M. Koperski, A. F. Morpurgo, and K. S. Novoselov, Magnetic 2D materials and heterostructures, Nat. Nanotechnol. **14**, 408 (2019).

[4] M.-C. Wang, C.-C. Huang, C.-H. Cheung, C.-Y. Chen, S. G. Tan, T.-W. Huang, Y. Zhao, Y. Zhao, G. Wu, Y.-P. Feng, H.-C. Wu, and C.-R. Chang, Prospects and opportunities of 2D van der Waals magnetic systems, Ann. Phys. **532**, 1900452 (2020).

[5] Y. Yao, X. Zhan, M. G. Sendeku, P. Yu, F. T. Dajan, C. Zhu, N. Li, J. Wang, F. Wang, Z. Wang, and J. He, Recent progress on emergent two-dimensional magnets and heterostructures, Nanotechnology **32**, 472001 (2021).

[6] Q. H. Wang, A. Bedoya-Pinto, M. Blei, A. H. Dismukes, A. Hamo, S. Jenkins, M. Koperski, Y. Liu, Q.-C. Sun, E. J. Telford, H. H. Kim, M. Augustin, U. Vool, J.-X. Yin, L. H. Li, A. Falin, C. R. Dean, F. Casanova, R. F. L. Evans, M. Chshiev *et al.*, The magnetic genome of two-dimensional van der Waals materials, ACS Nano **16**, 6960 (2022).

[7] L. Chen, J.-H. Chung, B. Gao, T. Chen, M. B. Stone, A. I. Kolesnikov, Q. Huang, and P. Dai, Topological Spin Excitations in Honeycomb Ferromagnet CrI_3, Phys. Rev. X **8**, 041028 (2018).

[8] L. Chen, J.-H. Chung, M. B. Stone, A. I. Kolesnikov, B. Winn, V. O. Garlea, D. L. Abernathy, B. Gao, M. Augustin, E. J. G. Santos, and P. Dai, Magnetic Field Effect on Topological Spin Excitations in CrI_3, Phys. Rev. X **11**, 031047 (2021).

[9] A. Mook, K. Plekhanov, J. Klinovaja, and D. Loss, Interaction-Stabilized Topological Magnon Insulator in Ferromagnets, Phys. Rev. X **11**, 021061 (2021).

[10] Z. Cai, S. Bao, Z.-L. Gu, Y.-P. Gao, Z. Ma, Y. Shangguan, W. Si, Z.-Y. Dong, W. Wang, Y. Wu, D. Lin, J. Wang, K. Ran, S. Li, D. Adroja, X. Xi, S.-L. Yu, X. Wu, J.-X. Li, and J. Wen, Topological magnon insulator spin excitations in the two-dimensional ferromagnet CrI_3, Phys. Rev. B **104**, L020402 (2021).

[11] Y. O. Kvashnin, A. Bergman, A. I. Lichtenstein, and M. I. Katsnelson, Relativistic exchange interactions in CrX_3 (X = Cl, Br, I), Phys. Rev. B **102**, 115162 (2020).

[12] R. Jaeschke-Ubiergo, E. Suarez Morell, and A. S. Nunez, Theory of magnetism in the van der Waals magnet CrI_3, Phys. Rev. B **103**, 174410 (2021).

[13] P. A. McClarty, Topological magnons: A review, Annu. Rev. Condens. Matter Phys. **13**, 171 (2022).

[14] K. Hejazi, Z.-X. Luo, and L. Balents, Noncollinear phases in moiré magnets, Proc. Natl. Acad. Sci. USA **117**, 10721 (2020).

[15] Y.-H. Li and R. Cheng, Moiré magnons in twisted bilayer magnets with collinear order, Phys. Rev. B **102**, 094404 (2020).

[16] C. Wang, Y. Gao, H. Lv, X. Xu, and D. Xiao, Stacking Domain Wall Magnons in Twisted Van Der Waals Magnets, Phys. Rev. Lett. **125**, 247201 (2020).

[17] H. Xie, X. Luo, G. Ye, Z. Ye, H. Ge, S. H. Sung, E. Rennich, S. Yan, Y. Fu, S. Tian, H. Lei, R. Hovden, K. Sun, R. He, and L. Zhao, Twist engineering of the two-dimensional magnetism in double bilayer chromium triiodide homostructures, Nat. Phys. **18**, 30 (2021).

[18] Y. Xu, A. Ray, Y.-T. Shao, S. Jiang, K. Lee, D. Weber, J. E. Goldberger, K. Watanabe, T. Taniguchi, D. A. Muller, K. F. Mak, and J. Shan, Coexisting ferromagnetic–antiferromagnetic state in twisted bilayer CrI_3, Nat. Nanotechnol. **17**, 143 (2021).

[19] F. Xiao and Q. Tong, Tunable strong magnetic anisotropy in two-dimensional van der Waals antiferromagnets, Nano Lett. **22**, 3946 (2022).

[20] F. Xiao, K. Chen, and Q. Tong, Magnetization textures in twisted bilayer CrX_3 (X = Br, I), Phys. Rev. Res. **3**, 013027 (2021).

[21] M. Akram, H. LaBollita, D. Dey, J. Kapeghian, O. Erten, and A. S. Botana, Moiré skyrmions and chiral magnetic phases in twisted CrX_3 (X = I, Br, and Cl) bilayers, Nano Lett. **21**, 6633 (2021).

[22] F. Zheng, Magnetic skyrmion lattices in a novel 2D-twisted bilayer magnet, Adv. Funct. Mater. **33**, 2206923 (2022).

[23] A. O. Fumega and J. L. Lado, Moiré-driven multiferroic order in twisted $CrCl_3$, $CrBr_3$ and CrI_3 bilayers, 2D Mater. **10**, 025026 (2023).

[24] B. Yang, Y. Li, H. Xiang, H. Lin, and B. Huang, Moiré magnetic exchange interactions in twisted magnets, Nat. Comput. Sci. **3**, 314 (2023).

[25] C. Xu, J. Feng, H. Xiang, and L. Bellaiche, Interplay between Kitaev interaction and single ion anisotropy in ferromagnetic CrI_3 and $CrGeTe_3$ monolayers, npj Comput. Mater. **4**, 57 (2018).

[26] C. Xu, J. Feng, M. Kawamura, Y. Yamaji, Y. Nahas, S. Prokhorenko, Y. Qi, H. Xiang, and L. Bellaiche, Possible Kitaev Quantum Spin Liquid State in 2D Materials with $S = 3/2$, Phys. Rev. Lett. **124**, 087205(R) (2020).

[27] C. Xu, J. Feng, S. Prokhorenko, Y. Nahas, H. Xiang, and L. Bellaiche, Topological spin texture in Janus monolayers of the chromium trihalides $Cr(I, X)_3$, Phys. Rev. B **101**, 060404(R) (2020).

[28] I. Lee, F. G. Utermohlen, D. Weber, K. Hwang, C. Zhang, J. van Tol, J. E. Goldberger, N. Trivedi, and P. C. Hammel, Fundamental Spin Interactions Underlying the Magnetic Anisotropy in the Kitaev Ferromagnet CrI_3, Phys. Rev. Lett. **124**, 017201 (2020).

[29] R. Yadav, L. Xu, M. Pizzochero, J. van den Brink, M. I. Katsnelson, and O. V. Yazyev, Electronic excitations and spin interactions in chromium trihalides from embedded many-body wave functions, arXiv:2208.02195.

[30] A. K. Geim and I. V. Grigorieva, Van der Waals heterostructures, Nature (London) **499**, 419 (2013).

[31] K. S. Novoselov, A. Mishchenko, A. Carvalho, and A. H. C. Neto, 2D materials and van der Waals heterostructures, Science **353**, aac9439 (2016).

[32] D. Zhong, K. L. Seyler, X. Linpeng, R. Cheng, N. Sivadas, B. Huang, E. Schmidgall, T. Taniguchi, K. Watanabe, M. A. McGuire, W. Yao, D. Xiao, K.-M. C. Fu, and X. Xu, Van der Waals engineering of ferromagnetic semiconductor heterostructures for spin and valleytronics, Sci. Adv. **3**, e1603113 (2017).

[33] T. Song, X. Cai, M. W.-Y. Tu, X. Zhang, B. Huang, N. P. Wilson, K. L. Seyler, L. Zhu, T. Taniguchi, K. Watanabe, M. A. McGuire, D. H. Cobden, D. Xiao, W. Yao, and X. Xu, Giant tunneling magnetoresistance in spin-filter van der Waals heterostructures, Science **360**, 1214 (2018).

[34] C. Cardoso, D. Soriano, N. A. García-Martínez, and J. Fernández-Rossier, Van der Waals Spin Valves, Phys. Rev. Lett. **121**, 067701 (2018).

[35] K. Zollner, P. E. Faria Junior, and J. Fabian, Proximity exchange effects in $MoSe_2$ and WSe_2 heterostructures with CrI_3: Twist angle, layer, and gate dependence, Phys. Rev. B **100**, 085128 (2019).

[36] Z. Wang, I. Gutiérrez-Lezama, N. Ubrig, M. Kroner, M. Gibertini, T. Taniguchi, K. Watanabe, A. Imamoğlu, E. Giannini, and A. F. Morpurgo, Very large tunneling magnetoresistance in layered magnetic semiconductor CrI_3, Nat. Commun **9**, 2516 (2018).

[37] H. H. Kim, B. Yang, T. Patel, F. Sfigakis, C. Li, S. Tian, H. Lei, and A. W. Tsen, One million percent tunnel magnetoresistance in a magnetic van der Waals heterostructure, Nano Lett. **18**, 4885 (2018).

[38] T. Song, M. W.-Y. Tu, C. Carnahan, X. Cai, T. Taniguchi, K. Watanabe, M. A. McGuire, D. H. Cobden, D. Xiao, W. Yao, and X. Xu, Voltage control of a van der Waals spin-filter magnetic tunnel junction, Nano Lett. **19**, 915 (2019).

[39] S. Rahman, J. F. Torres, A. R. Khan, and Y. Lu, Recent developments in van der Waals antiferromagnetic 2D materials: Synthesis, characterization, and device implementation, ACS Nano **15**, 17175 (2021).

[40] M.-C. Heißenbüttel, T. Deilmann, P. Krüger, and M. Rohlfing, Valley-dependent interlayer excitons in magnetic WSe_2CrI_3, Nano Lett. **21**, 5173 (2021).

[41] B. Huang, G. Clark, E. Navarro-Moratalla, D. R. Klein, R. Cheng, K. L. Seyler, D. Zhong, E. Schmidgall, M. A. McGuire, D. H. Cobden, W. Yao, D. Xiao, P. Jarillo-Herrero, and X. Xu, Layer-dependent ferromagnetism in a van der Waals crystal down to the monolayer limit, Nature (London) **546**, 270 (2017).

[42] B. Huang, G. Clark, D. R. Klein, D. MacNeill, E. Navarro-Moratalla, K. L. Seyler, N. Wilson, M. A. McGuire, D. H. Cobden, D. Xiao, W. Yao, P. Jarillo-Herrero, and X. Xu, Electrical control of 2D magnetism in bilayer CrI_3, Nat. Nanotechnol. **13**, 544 (2018).

[43] D. R. Klein, D. MacNeill, J. L. Lado, D. Soriano, E. Navarro-Moratalla, K. Watanabe, T. Taniguchi, S. Manni, P. Canfield, J. Fernández-Rossier, and P. Jarillo-Herrero, Probing magnetism in 2D van der Waals crystalline insulators via electron tunneling, Science **360**, 1218 (2018).

[44] W. Chen, Z. Sun, Z. Wang, L. Gu, X. Xu, S. Wu, and C. Gao, Direct observation of van der Waals stacking–dependent interlayer magnetism, Science **366**, 983 (2019).

[45] H. H. Kim, B. Yang, S. Li, S. Jiang, C. Jin, Z. Tao, G. Nichols, F. Sfigakis, S. Zhong, C. Li, S. Tian, D. G. Cory, G.-X. Miao, J. Shan, K. F. Mak, H. Lei, K. Sun, L. Zhao, and A. W. Tsen, Evolution of interlayer and intralayer magnetism in three atomically thin chromium trihalides, Proc. Natl. Acad. Sci. USA **116**, 11131 (2019).

[46] D. R. Klein, D. MacNeill, Q. Song, D. T. Larson, S. Fang, M. Xu, R. A. Ribeiro, P. C. Canfield, E. Kaxiras, R. Comin, and P. Jarillo-Herrero, Enhancement of interlayer exchange in an ultrathin two-dimensional magnet, Nat. Phys. **15**, 1255 (2019).

[47] T. Li, S. Jiang, N. Sivadas, Z. Wang, Y. Xu, D. Weber, J. E. Goldberger, K. Watanabe, T. Taniguchi, C. J. Fennie, K. F. Mak, and J. Shan, Pressure-controlled interlayer magnetism in atomically thin CrI_3, Nat. Mater. **18**, 1303 (2019).

[48] X. Guo, W. Jin, Z. Ye, G. Ye, H. Xie, B. Yang, H. H. Kim, S. Yan, Y. Fu, S. Tian, H. Lei, A. W. Tsen, K. Sun, J.-A. Yan, R. He, and L. Zhao, Structural monoclinicity and its coupling to layered magnetism in few-layer CrI_3, ACS Nano **15**, 10444 (2021).

[49] G. Cheng, M. M. Rahman, A. L. Allcca, A. Rustagi, X. Liu, L. Liu, L. Fu, Y. Zhu, Z. Mao, K. Watanabe, T. Taniguchi, P. Upadhyaya, and Y. P. Chen, Electrically tunable moiré magnetism in twisted double bilayers of chromium triiodide, Nat. Electron (2023).

[50] H. Xie, X. Luo, Z. Ye, Z. Sun, G. Ye, S. H. Sung, H. Ge, S. Yan, Y. Fu, S. Tian, H. Lei, K. Sun, R. Hovden, R. He, and L. Zhao, Evidence of non-collinear spin texture in magnetic moiré superlattices, Nat. Phys. (2023).

[51] N. Sivadas, S. Okamoto, X. Xu, C. J. Fennie, and D. Xiao, Stacking-dependent magnetism in bilayer CrI_3, Nano Lett. **18**, 7658 (2018).

[52] D. Soriano, C. Cardoso, and J. Fernández-Rossier, Interplay between interlayer exchange and stacking in CrI_3 bilayers, Solid State Commun. **299**, 113662 (2019).

[53] S. W. Jang, M. Y. Jeong, H. Yoon, S. Ryee, and M. J. Han, Microscopic understanding of magnetic interactions in bilayer CrI_3, Phys. Rev. Mater. **3**, 031001(R) (2019).

[54] P. Jiang, C. Wang, D. Chen, Z. Zhong, Z. Yuan, Z.-Y. Lu, and W. Ji, Stacking tunable interlayer magnetism in bilayer CrI_3, Phys. Rev. B **99**, 144401 (2019).

[55] M. Gibertini, Magnetism and stability of all primitive stacking patterns in bilayer chromium trihalides, J. Phys. D **54**, 064002 (2020).

[56] D. Soriano, M. I. Katsnelson, and J. Fernández-Rossier, Magnetic two-dimensional chromium trihalides: A theoretical perspective, Nano Lett. **20**, 6225 (2020).

[57] S. Sarkar and P. Kratzer, Magnetic exchange interactions in bilayer CrX_3 (X = Cl, Br, and I): A critical assessment of the DFT + u approach, Phys. Rev. B **103**, 224421 (2021).

[58] D. Wang and B. Sanyal, Systematic study of monolayer to trilayer CrI_3: Stacking sequence dependence of electronic structure and magnetism, J. Phys. Chem. C **125**, 18467 (2021).

[59] H. Yu, J. Zhao, and F. Zheng, Interlayer magnetic interactions in $\pi/3$-twisted bilayer CrI_3, Appl. Phys. Lett. **119**, 222403 (2021).

[60] S. Stavrić, P. Barone, and S. Picozzi, Delving into the anisotropic interlayer exchange in bilayer CrI_3, arXiv:2305.16142.

[61] P. W. Anderson, Antiferromagnetism. Theory of superexchange interaction, Phys. Rev. **79**, 350 (1950).

[62] P. W. Anderson, New approach to the theory of superexchange interactions, Phys. Rev. **115**, 2 (1959).

[63] K. W. Song and V. I. Fal'ko, Superexchange and spin-orbit coupling in monolayer and bilayer chromium trihalides, Phys. Rev. B **106**, 245111 (2022).

[64] The local spin wave function with opposite spin direction ($-\mathbf{s}_\mathbf{r}$) is $\chi^{\ell-}_{\mathbf{r}\sigma} = \sum_{\sigma'} i\tau^y_{\sigma\sigma'}\bar{\chi}^{\ell+}_{\mathbf{r}\sigma'}$.

[65] R. Shankar, Renormalization-group approach to interacting fermions, Rev. Mod. Phys. **66**, 129 (1994).

[66] See Supplemental Material at http://link.aps.org/supplemental/10.1103/PhysRevB.107.245133 for derivations and computational details.

[67] F. Guinea and N. R. Walet, Continuum models for twisted bilayer graphene: Effect of lattice deformation and hopping parameters, Phys. Rev. B **99**, 205134 (2019).

[68] P. Giannozzi, O. Andreussi, T. Brumme, O. Bunau, M. B. Nardelli, M. Calandra, R. Car, C. Cavazzoni, D. Ceresoli, M. Cococcioni, N. Colonna, I. Carnimeo, A. D. Corso, S. de Gironcoli, P. Delugas, R. A. DiStasio, A. Ferretti, A. Floris, G. Fratesi, G. Fugallo *et al.*, Advanced capabilities for materials modelling with Quantum ESPRESSO, J. Phys. Condens. Matter. **29**, 465901 (2017).

[69] N. Marzari, A. A. Mostofi, J. R. Yates, I. Souza, and D. Vanderbilt, Maximally localized Wannier functions: Theory and applications, Rev. Mod. Phys. **84**, 1419 (2012).

[70] G. Pizzi, V. Vitale, R. Arita, S. Blügel, F. Freimuth, G. Géranton, M. Gibertini, D. Gresch, C. Johnson, T. Koretsune, J. Ibañez-Azpiroz, H. Lee, J.-M. Lihm, D. Marchand, A. Marrazzo, Y. Mokrousov, J. I. Mustafa, Y. Nohara, Y. Nomura, L. Paulatto *et al.*, Wannier90 as a community code: New features and applications, J. Phys.: Condens. Matter. **32**, 165902 (2020).

[71] K. Lejaeghere, G. Bihlmayer, T. Björkman, P. Blaha, S. Blügel, V. Blum, D. Caliste, I. E. Castelli, S. J. Clark, A. D. Corso, S. de Gironcoli, T. Deutsch, J. K. Dewhurst, I. D. Marco, C. Draxl, M. Dułak, O. Eriksson, J. A. Flores-Livas, K. F. Garrity, L. Genovese, Reproducibility in density functional theory calculations of solids, Science **351**, aad3000 (2016).

[72] G. Prandini, A. Marrazzo, I. E. Castelli, N. Mounet, and N. Marzari, Precision and efficiency in solid-state pseudopotential calculations, npj Comput. Mater **4**, 72 (2018).

[73] S. Fang, R. Kuate Defo, S. N. Shirodkar, S. Lieu, G. A. Tritsaris, and E. Kaxiras, *Ab initio* tight-binding Hamiltonian for transition metal dichalcogenides, Phys. Rev. B **92**, 205108 (2015).

[74] M. Wu, Z. Li, T. Cao, and S. G. Louie, Physical origin of giant excitonic and magneto-optical responses in two-dimensional ferromagnetic insulators, Nat. Commun. **10**, 12371 (2019).

[75] S. Acharya, D. Pashov, B. Cunningham, A. N. Rudenko, M. Rösner, M. Grüning, M. van Schilfgaarde, and M. I. Katsnelson, Electronic structure of chromium trihalides beyond density functional theory, Phys. Rev. B **104**, 155109 (2021).

[76] V. Fiorentini and A. Baldereschi, Dielectric scaling of the self-energy scissor operator in semiconductors and insulators, Phys. Rev. B **51**, 17196 (1995).

[77] K. A. Johnson and N. W. Ashcroft, Corrections to density-functional theory band gaps, Phys. Rev. B **58**, 15548 (1998).

[78] N. Bernstein, M. J. Mehl, and D. A. Papaconstantopoulos, Nonorthogonal tight-binding model for germanium, Phys. Rev. B **66**, 075212 (2002).

[79] S. J. Magorrian, V. Zólyomi, and V. I. Fal'ko, Electronic and optical properties of two-dimensional InSe from a DFT-parametrized tight-binding model, Phys. Rev. B **94**, 245431 (2016).

[80] W.-B. Zhang, Q. Qu, P. Zhu, and C.-H. Lam, Robust intrinsic ferromagnetism and half semiconductivity in stable two-dimensional single-layer chromium trihalides, J. Mater. Chem. C **3**, 12457 (2015).

[81] J. L. Lado and J. Fernández-Rossier, On the origin of magnetic anisotropy in two dimensional CrI_3, 2D Mater. **4**, 035002 (2017).

[82] O. Besbes, S. Nikolaev, N. Meskini, and I. Solovyev, Microscopic origin of ferromagnetism in the trihalides $CrCl_3$ and CrI_3, Phys. Rev. B **99**, 104432 (2019).

[83] D. Torelli, K. S. Thygesen, and T. Olsen, High throughput computational screening for 2D ferromagnetic materials: The critical role of anisotropy and local correlations, 2D Mater. **6**, 045018 (2019).

[84] Z. Wu, J. Yu, and S. Yuan, Strain-tunable magnetic and electronic properties of monolayer CrI_3, Phys. Chem. Chem. Phys. **21**, 7750 (2019).

[85] I. V. Kashin, V. V. Mazurenko, M. I. Katsnelson, and A. N. Rudenko, Orbitally-resolved ferromagnetism of monolayer CrI_3, 2D Mater. **7**, 025036 (2020).

[86] P. P. Stavropoulos, X. Liu, and H.-Y. Kee, Magnetic anisotropy in spin-3/2 with heavy ligand in honeycomb Mott insulators: Application to CrI_3, Phys. Rev. Res. **3**, 013216 (2021).

[87] T. Moriya, Anisotropic superexchange interaction and weak ferromagnetism, Phys. Rev. **120**, 91 (1960).

[88] The analytical expression is similar to interlayer DM interaction by replacing $T_{12}^{\ell_1\ell_2} \to v_{12}$. Using $\lambda = 0.6$ eV [81], we estimate the interactions between AA sublattices through the h_2-h_5 hopping $\boldsymbol{\mathcal{D}}'_{\rm AA} = (-0.05, 0.01, -0.09)$, and between BB sublattices h_1-h_6 hopping $\boldsymbol{\mathcal{D}}'_{\rm BB} = (0.05, -0.01, 0.09)$ in meV [see Fig. 1(a)]. The result is consistent with Refs. [11,27]. The DM vectors are pointing along the X-X bond direction.

[89] The analytical result can be found in SM [66].

[90] J. B. Goodenough, An interpretation of the magnetic properties of the perovskite-type mixed crystals $La_{1-x}Sr_xCoO_{3-\lambda}$, J. Phys. Chem. Solids **6**, 287 (1958).

[91] J. Kanamori, Superexchange interaction and symmetry properties of electron orbitals, J. Phys. Chem. Solids **10**, 87 (1959).

[92] Specifically, in Figs. 1(c) and 1(d), sliding does not change the relative orientation between the red dashed triangles in the upper and lower layers. As we see in Figs. 3 and 4, this can lead to a qualitative change in the interlayer exchange.